© 2019. Published by The Company of Biologists Ltd | Journal of Cell Science (2019) 132, jcs232058. doi:10.1242/jcs.232058

RESEARCH ARTICLE

Mannose glycosylation is an integral step for NIS localization and function in human breast cancer cells

Maitreyi Rathod[1,3,‡], Sushmita Chatterjee[1,‡], Shruti Dutta[1], Rajiv Kalraiya[2,3,§], Dibyendu Bhattacharyya[4,3] and Abhijit De[1,3,¶]

ABSTRACT

Chasing an intriguing biological question on the disparity of sodium iodide symporter (NIS, officially known as SLC5A5) expression and function in the clinical scenario of breast cancer, this study addresses key molecular defects involved. NIS in cancer patients has primarily been recorded to be a cytoplasmic protein, thus limiting the scope for targeted radio-iodine therapy. We developed NIS transgene-overexpressing MCF-7 breast cancer cells, and found a few clonal derivatives that show predominant expression of NIS in the plasma membrane. The majority of clones, however, showed cytosolic NIS expression over long passages. Cells expressing membranous NIS show unperturbed dynamic trafficking of NIS through secretory pathway organelles when compared to cells expressing cytoplasmic NIS or to parental cells. Further, treatment of cells expressing membranous NIS with specific glycosylation inhibitors highlighted the importance of inherent glycosylation processing and an 84 gene signature glycosylation RT-Profiler array revealed that clones expressing NIS in their membrane cluster separately compared to the other cells. We further confirm a role of three differentially expressed genes, i.e. *MAN1B1*, *MAN1A1* and *MAN2A1*, in regulating NIS localization by RNA interference. Thus, this study shows the important role of mannosidase in N-glycosylation processing in order to correctly traffic NIS to the plasma membrane in breast cancer cells.

This article has an associated First Person interview with the first author of the paper.

KEY WORDS: Sodium iodide symporter, NIS, SLC5A5, Protein trafficking, Glycosylation, Mannosidase, Breast cancer

INTRODUCTION

In humans, sodium iodide symporter (NIS, officially known as SLC5A5) is the sole iodine pump protein present in certain cells – such as thyroid follicular cells, gastric mucosa, salivary gland or even lactating mammary gland cells – where iodine transport through the cell barrier is important for normal organ function and physiology (Riedel et al., 2001a). As a member of a solute carrier family of proteins, its localization on cell membrane is important for its function and, possibly, governed by three putative N-linked glycosylation sites at amino acid positions 225, 485 and 497 (Levy et al., 1997). Abundant overexpression (80% positive cases) of NIS in breast cancer has been reported worldwide (Chatterjee et al., 2013; Ryan et al., 2011; Tazebay et al., 2000; Wapnir et al., 2003), raising a hope of utilizing this endogenous protein in targeted radio-iodine-based diagnostic imaging and/or therapy for patients. But, over time, insufficient NIS levels on the plasma membrane proved to be the bottleneck (Dutta and De, 2015). By using immunohistochemistry to study NIS, is has been revealed that the majority of breast cancer tissue shows cytoplasmic expression of NIS, whereas control staining of normal thyroid or salivary gland with the same monoclonal antibody shows the typical membrane staining (Chatterjee et al., 2013). One important study with a particular focus on analyzing the subcellular localization of NIS has shown that, among all the positive breast cancer tissue specimens, only 27% cases represented membrane localization (Beyer et al., 2009). In fact, this study related the subcellular expression of NIS to the disappointing clinical imaging results, which showed only 17–25% of breast cancer patients with visible radionuclide uptake (Moon et al., 2001). Later, the same was confirmed by many others, including us (Chatterjee et al., 2013; Renier et al., 2009).

To address this limitation, studies have attempted to identify factors responsible for the membrane localization of NIS (Chung et al., 2015; Riedel et al., 2001b). Glycosylation is a post-translational modification (PTM) that controls many biological processes, such as protein folding, stability or subcellular localization of proteins (Zhou et al., 2005). Defects in N-linked glycosylation have been shown to be associated with impaired cell surface expression of some membrane transporters (Weng et al., 2013). The primary site for N-linked glycosylation in the cell is the endoplasmic reticulum (ER), where the core glycan attaches to the dolichol phosphate anchor in the lumen of the ER and is further processed for folding. ER-resident chaperons, such as calnexin and calreticulin, assist in recognizing the misfolded proteins and then recruit other folding chaperons, e.g. PDI, which helps in protein folding (Benyair et al., 2015). Folded proteins are then allowed to exit the ER and enter the Golgi complex, where maturation of glycoproteins takes place by final processing of N-glycans that are generating either hybrid, complex or mannose-rich type glycans. Only the mature form of proteins then migrate to their destination (Aebi, 2013; Parodi, 2000). Thus, glycan maturation and subsequent modifications are important for folding and intracellular trafficking of glycoproteins. Since the localization of NIS in the majority of breast cancer cases is defective, we here study the dynamic distribution within primary cellular compartments.

Past studies have shown that in T47D breast cancer cells, where NIS is predominantly present in the cytoplasm, EGF-mediated ERK

[1]Molecular Functional Imaging Laboratory, ACTREC, Tata Memorial Centre, Navi Mumbai, Maharashtra 410210, India. [2]Glycobiology Laboratory, ACTREC, Tata Memorial Centre, Navi Mumbai, Maharashtra 410210, India. [3]Homi Bhabha National Institute, Anushakti Nagar, Mumbai, India. [4]Cell Imaging Laboratory, ACTREC, Tata Memorial Centre, Navi Mumbai, Maharashtra 410210, India.

‡These authors contributed equally to this work
§Deceased

¶Author for correspondence (ade@actrec.gov.in)

S.C., 0000-0002-2975-4346; S.D., 0000-0003-4630-239X; D.B., 0000-0003-3252-7440; A.D., 0000-0002-5818-0206

Received 19 March 2019; Accepted 21 August 2019

Journal of Cell Science (2019) 132, jcs232058. doi:10.1242/jcs.232058

activation improves membrane localization of this transporter and, thus, enhances its function (Jung et al., 2008). Another study has shown PI3K activation to negatively regulate NIS glycosylation and function (Knostman et al., 2007). Treatment of cells with tunicamycin to inhibit the first step of glycosylation shows a dramatic reduction of membrane-localized NIS and accumulation of a 55 kDa de-glycosylated form of NIS – as shown by immunoblotting (Beyer et al., 2011; Chung et al., 2015). Combined mutation of the three putative sites of N-linked glycosylation have shown an ∼50% reduction in the function of NIS isolated from rat thyroid tissue (Levy et al., 1998), and an >50% reduction in its in function in human breast cancer cells (Beyer et al., 2011). In addition, treatment of cells with KT5823, a staurosporine-related protein kinase inhibitor, leads to an accumulation of hypo-glycosylated NIS in the cytoplasm (Beyer et al., 2011), thus, highlighting the role of glycosylation as an important PTM that dictates the function of NIS (Chung et al., 2015). Defective localization of NIS in the cytoplasm due to mutations, such as for R124H NIS have been reported in COS cells (Paroder et al., 2013). Further, these authors have also shown that the R124H NIS mutant is retained within cytoplasmic ER and incapable of localizing to the Golgi (Paroder et al., 2013). Although N-linked glycosylation has been suggested as a mediator that regulates NIS localization, effector molecules affecting this process remained unidentified. Therefore, to better understand defective localization of NIS in breast cancer cells, we report the development and use of clones derived from a breast cancer cell line, which show a different localization of NIS, and further identify the key processing genes responsible. This multi-parametric investigation reveals novel information on impaired cellular trafficking processes of NIS and will have main implications on our understanding of the localization and function of this iodine pump protein.

RESULTS

Defective membrane localization of NIS is linked to impaired trafficking within breast adenocarcinoma cells

To verify whether NIS localization to the cell membrane is linked to cellular protein trafficking, we tracked endogenous NIS protein through reporter-tagged intracellular secretary pathway organelles. Proteins destined for the plasma membrane are folded in the endoplasmic reticulum (ER) followed by maturation in the Golgi complex. Hence, the presence of NIS in the ER, ER exit sites and Golgi complex was tracked using GFP-tagged KDEL, Sec16B and GalNac T2 molecular marker proteins, respectively (Connerly et al., 2005; Love et al., 1998; Munro and Pelham, 1987). MCF-7 breast cancer cells (hereafter referred to as baseline MCF-7 cells) all express a detectable amount of NIS protein and were treated with brefeldin A (BFA) for 30 min causing complete disruption of the Golgi complex, which was restored rather slowly within 12 h after BFA was withdrawn (Fig. S1A,B). Disruption of the Golgi led to accumulation of cargo (i.e. NIS) in the ER and, when the Golgi was restored, cargo trafficking from ER to Golgi was tracked by the colocalization of NIS with respective organelle markers. NIS colocalization with the ER, ER exit site or Golgi at 0 h, 6 h and 12 h post BFA treatment are shown in Fig. 1A. Over time NIS was able to enter ER exit sites and, thus, the overlap coefficients of NIS and ER exit sites slightly increased from 0.5 (0 h) to 0.6 (12 h). At the 0 h time point, i.e. the time at which the Golgi complex was completely disrupted, Golgi-resident cargo moved to the ER through retrograde transport. Hence, the staining pattern of NIS with GalNac T2 at this time mimics that of NIS with ER (Fig. 1A). But, interestingly, with time the colocalization signal for NIS with GalNac T2 dropped significantly (P=0.0001), indicating a defective transport of NIS in

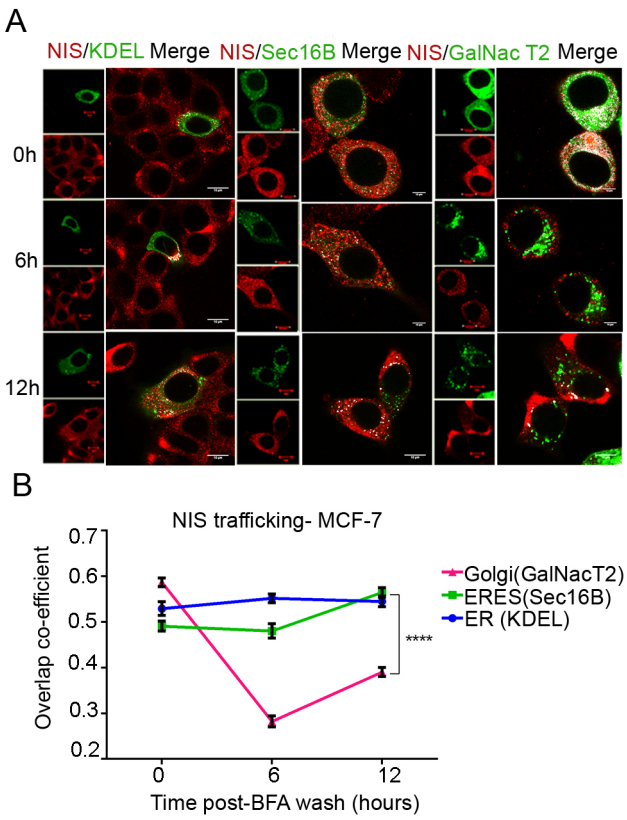

Fig. 1. Baseline MCF-7 cells show defective NIS trafficking through secretory pathway. (A) Colocalization of NIS with the ER marker KDEL, the ER exit site (ERES) marker Sec-16B or the Golgi marker GalNac T2. Red indicates NIS stained with anti-mouse Dylight 633 secondary antibody; green represents organelle-specific markers fused to GFP reporter. 0 h, 6 and 12 h indicate time points after BFA rescue (i.e. the course of Golgi restoration). The images represent a single plane. White spots on the merge channel show colocalization between the two channels. Scale bars: 10 µm. Images were acquired using a 63× objective with oil. (B) Graph showing overlap coefficients of NIS (red) with GalNac T2, KDEL (blue) or Sec-16B (green) at 0 h, 6 h and 12 h after treatment with BFA. Error bars indicate ±s.e.m. ****P<0.0001.

baseline MCF-7 cells. Results obtained by quantifying the overlap coefficient values indicated that NIS remains colocalized in the ER compartment at all time (Fig. 1B). Additionally, another endogenous glycoprotein, EGFR, is similarly tracked in MCF-7 cells, where it can cross ER exit sites (ERES) (Fig. S2A,B).

MCF-7 clonal cells that overexpress NIS show a different localization pattern of the protein

To investigate the intracellular trafficking defect of NIS, we developed a NIS-overexpressing MCF-7 cell (hereafter referred to as MCF-7 clonal cells) by transfecting a bi-cistronic plasmid expression vector that consists of the β-actin promoter driving the human NIS DNA and IRES-TurboFP.Fluc2. The cap-dependent translation of NIS and the cap independent translation of the TurboFP.Fluc2 fusion reporter help to achieve simultaneous expression of NIS and the fusion reporter genes (Fig. 2A). MCF-7 clonal cells, with 10-1000 fold higher luciferase activity were selected (Fig. 2B), and further cross-verified for NIS expression by immunofluorescence (IF). Strikingly, out of all 37 NIS-positive clones screened, only six clones showed NIS protein localized at the cell membrane (i.e. cl2, cl22, cl30, cl31, cl32, cl34), whereas the remaining clones showed cytoplasmic localization similar to that of

Journal of Cell Science (2019) 132, jcs232058. doi:10.1242/jcs.232058

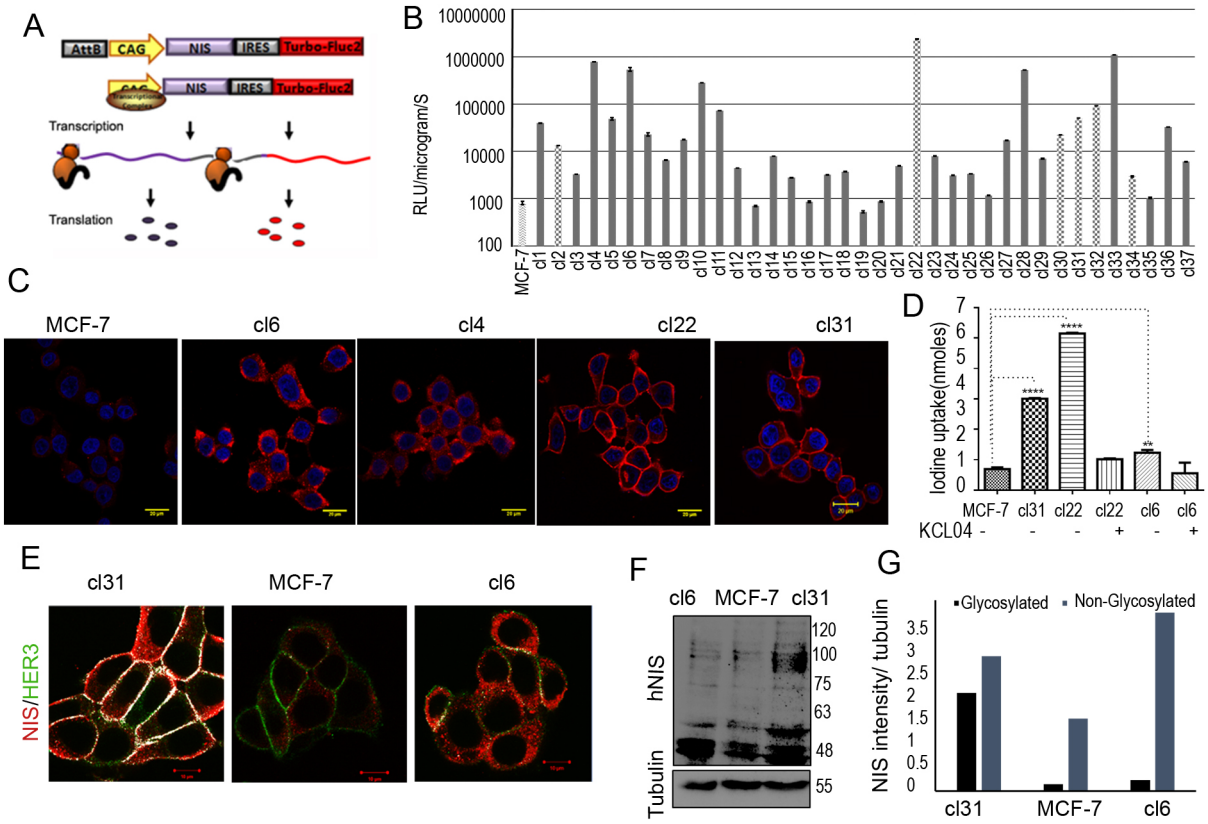

Fig. 2. Generation of NIS-overexpressing MCF-7 cell clones with different localizations of NIS. (A) The bi-cistronic plasmid vector used in the study. The therapeutic gene (human NIS) and the fusion reporter gene (TurboFp.Fluc2) are linked through an EMCV-IRES sequence, which allows translation of the second cistron. (B) Bar graph representing screening of MCF-7 clones on the basis of their luciferase expression measures in RLU/microgram/S (relative light units/µg/second); patterned bars represent clones with distinct NIS expression on the cell membrane, which was verified by IF. (C) Photomicrographs of some MCF-7 cell clones after NIS IF (red) and cross staining with DAPI (blue), showing marked differences in NIS localization, i.e. cytoplasmic or membranous (cl6 and cl4 or cl22 and cl31, respectively) compared to that in untransfected MCF-7 cells. Scale bars: 20 µm. (D) Iodide uptake assay in MCF-7 NIS-expressing clones. Blocking of NIS with perchlorate shows significant decrease in iodide uptake, indicating NIS specific uptake. $^{**}P<0.01$, $^{****}P<0.0001$. (E) Photomicrographs of baseline MCF-7, cl31 and cl6 cells that had undergone double-IF, staining for NIS (red) and Her3 (green). Scale bars: 10 µm. (F) Western blot showing completely glycosylated (100 kDa), partially glycosylated (65 kDa) and non-glycosylated (50 kDa) NIS in cl31, cl6 and MCF-7 cells. (G) Densitometric analysis of glycosylated and non-glycosylated NIS normalized to tubulin (loading control) in cl31, cl6 and MCF-7 cells.

baseline MCF-7 cells (Fig. 2C). The MCF-7 cell line is known to have high endogenous expression of the HER3 receptor (officially known as ERBB3). Therefore, double-IF staining for NIS and HER3 was performed in representative clones to further confirm our observation on NIS localization differences (Fig. 2E). Following this interesting finding of differently localized NIS in clonal cells, we have rigorously followed their reporter and NIS expression over ten serial passages for two clonal cell populations of each type – i.e. cl22 and cl31 for membrane NIS and cl4 and cl6 for cytoplasmic NIS – to ensure that the respective pattern is maintained (Fig. S3A–D). To reveal the intensity of NIS expression in clonal cells, immunoblotting was performed, This shows a higher amount of fully glycosylated (100 kDa) NIS in cl31 compared with the cl6 (cytoplasmic NIS) and baseline MCF-7 cells (Fig. 2F,G). We have also performed karyotyping (GTG banding) of baseline MCF-7 cells and of representative clonal cell variants. We also found a near-triploidy karyotype and similar abnormalities, such as a derivative chromosome 1, and isochromosomes of 7 and 11. However, apart from resembling the parental karyotype, the clones do show a few karyotypic differences, such as deletions and extra copies of some chromosomes (see Table S1). It should also be noticed that chromosome 19, which carries the NIS gene in humans, is unaltered across all cells. These results, therefore, indicate that clonal heterogeneity lies within the MCF-7 cell population, which might have an effect on different localizations of the target.

Further, we tried to verify whether localization of NIS at the plasma membrane of cl31 dictates its function, and a non-radioactive iodine uptake assay was performed as described (Kelkar et al., 2016). As expected, those cells expressing NIS at the membrane showed a significantly higher (P=0.002) uptake of iodine compared with those expressing it in the cytoplasm (Fig. 2D). Uptake of iodine was significantly reduced in response to inhibition with perchlorate, indicating assay specificity. Together, by introducing a NIS-containing transgene in MCF-7 cells, we established two distinctly different clonal cell derivatives, one with NIS appropriately localized at the cell surface and the other with mislocalized protein. These cellular features are well maintained over multiple passages and show clear differences in terms of iodine pump function.

NIS protein trafficking follows a conventional pathway in clonal cells with membrane localization of NIS

The clonal variants of MCF-7 cells that overexpress NIS (clonal cells) at the plasma membrane provide a unique opportunity to verify whether NIS follows the classic intracellular trafficking pathway. Following a strategy similar to the one described above,

Journal of Cell Science (2019) 132, jcs232058. doi:10.1242/jcs.232058

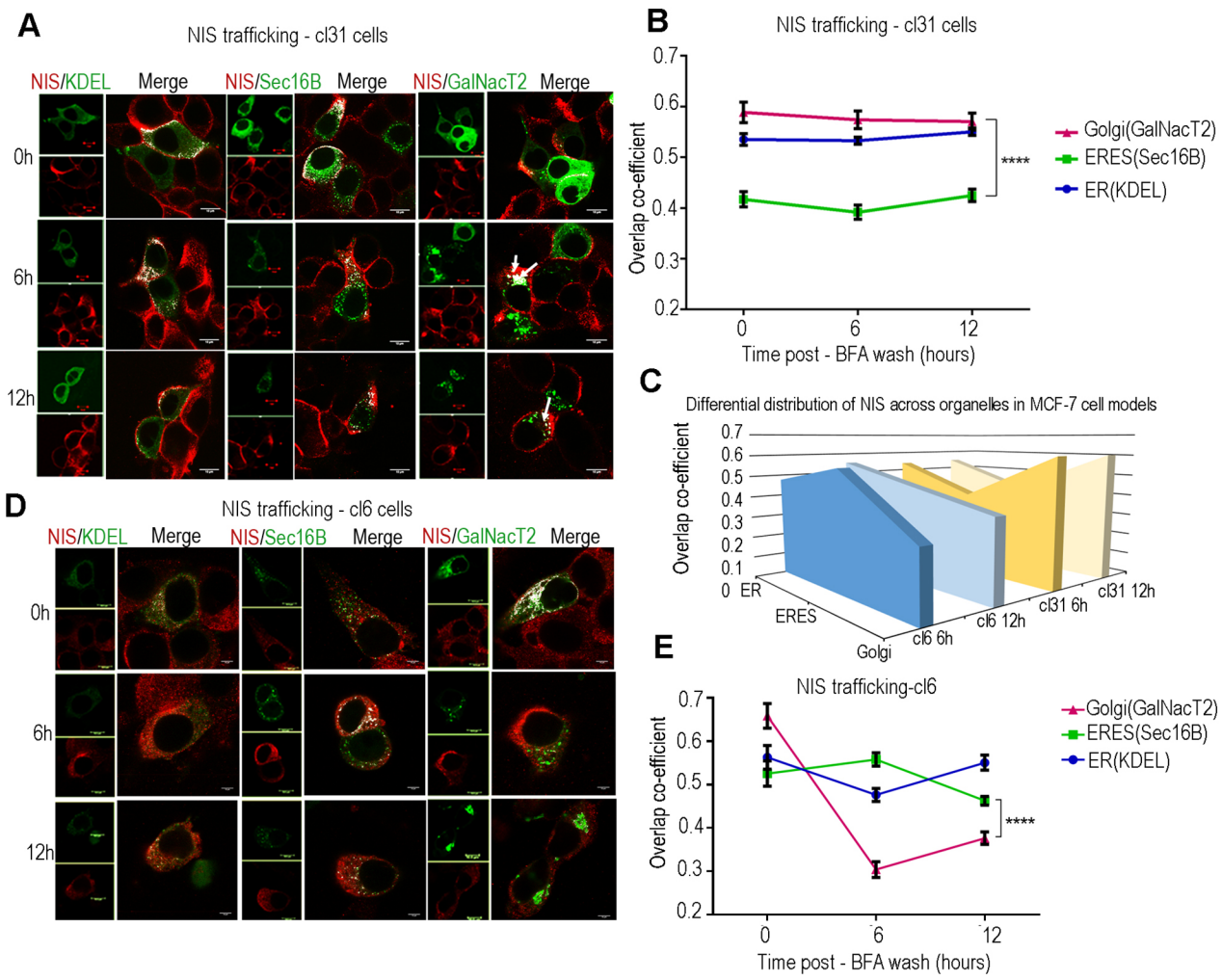

Fig. 3. MCF-7 clonal cells cl31 and cl6 cells show different NIS trafficking via the secretory pathway. (A,D) Micrographs, showing colocalization of NIS (red) with KDEL, sec-16B or GalNac T2 (green) in cl31 (A) and cl6 (D) cells. All images represent a single plane. White spots are points of colocalization. Scale bars: 10 µm. White arrows indicate colocalization of NIS and the Golgi marker to compare cl31 and cl6 cells. (B,E) Average overlap of coefficients obtained for NIS with GalNac T2, KDEL or Sec-16B markers in cl31 (B) and cl6 (E) cells. The best middle plane was used for quantification. Error bars indicate s.e.m. ****P<0.0001. (C) Distribution of NIS from ER via ERES to the Golgi complex as the Golgi is restored in cl31 and cl6 cells; y-axis values indicate the average overlap coefficient values of NIS and the respective organelle marker.

the overlap coefficient of NIS and ER maintains a value of 0.55 in cl31 cells after treatment with BFA (Fig. 3A,B). Additionally, during disrupted Golgi transport at 0 h, with an overlap coefficient value of 0.53, the coefficient value goes up to 0.6 over time as Golgi is restored. This indicates that NIS is capable to traffic normally as the Golgi is restored in cells where the pump protein is properly placed on the membrane. In comparison, NIS-overexpressing cytoplasmic clone (cl6), we find that intracellular trafficking pattern resembles more that of parental MCF-7 cell. The overlap coefficient of NIS with ER slightly increases from 0.47 (6 h) to 0.55 (12 h). Later, 12 h after BFA treatment, when the restoration of the Golgi structure is complete, the overlap value of NIS with an intact Golgi is markedly lower, with a coefficient of 0.3 (Fig. 3D,E). For ER exit sites, NIS colocalization with the sec16B marker shows coefficient values of 0.52 (0 h) and 0.558 (6 h), which reduces to 0.46 (12 h). Therefore, in the cytoplasmic clone, limited NIS trafficking to Golgi is implicated. Thus, the overall distribution of NIS across main organelles is depicted in Fig. 3C. It reveals that in cells that express NIS at the membrane, NIS traffic from ER to Golgi increases over time and progresses normally as the Golgi is restored. In cells that express NIS at the cytoplasm, NIS remains accumulated in the ER and/or ERES, as trafficking to the Golgi is greatly affected. Parallel protein trafficking experiments for the EGFR was also carried out by using the same clonal cell types. Compared to cl6, cl31 cells here show significantly higher (P=0.005) amounts of EGFR in the Golgi within 6 h after treatment with BFA (Fig. S2C).

NIS association with calnexin is increased in cells with defective trafficking

The association of proteins with folding chaperons, such as calnexin, can provide insights into their folding state, as well as the quality of newly synthesized glycoproteins. The association of NIS with calnexin was measured by IF in the two clonal cell types. For this, baseline MCF-7 and clonal cell derivatives were treated with cyclohexamide (chx) to inhibit translation for 12 h until fully glycosylated NIS protein becomes undetectable. After a short rescue period (6 h), cells were fixed and stained with antibodies against NIS and calnexin to capture their association. The overlap coefficient obtained in cl31 was significantly lower (P<0.05) than in cl6 or baseline MCF-7 cells, indicating that the nascent NIS

Journal of Cell Science (2019) 132, jcs232058. doi:10.1242/jcs.232058

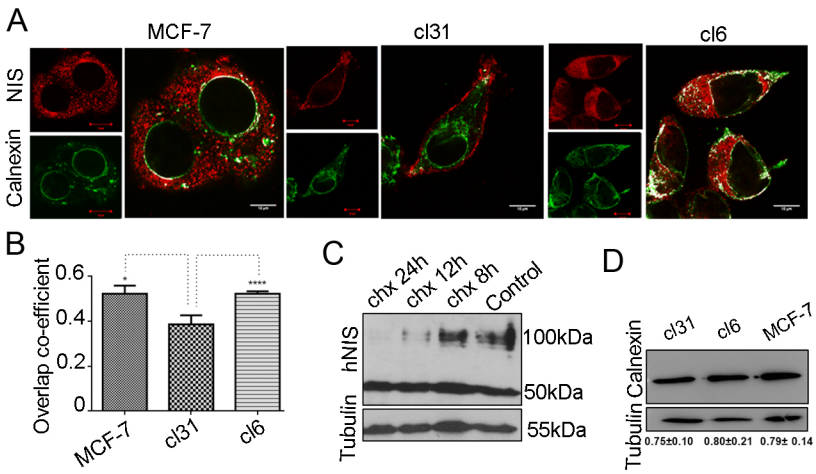

Fig. 4. NIS shows a higher association with calnexin in cells with trafficking defect. (A) Immunofluorescence images showing the colocalization of calnexin (green) with NIS (red) in cl31, cl6 and MCF-7 cells. Binary vision (white spots) indicates points of colocalization between NIS and calnexin. The images show a single best plane. Scale bars: 10 µm. (B) Bar graph showing the calculated overlap coefficients between NIS and calnexin. The association in cl6 cells is significantly higher (P<0.0001) when compared to cl31 cells. Error bars represent +s.e.m; *P<0.05; ****P<0.0001. (C) Western blot showing the decrease of NIS protein levels at different time points in response to treatment with chx. (D) Western blot showing calnexin protein levels in cl31, cl6 and MCF-7 cells. Tubulin was used as a loading control.

molecule is in a folding-competent state, thus, enabling correct membrane localization of NIS in cl31 (Fig. 4A,B). Interestingly, in the chx-treatment, cl31 cells showed that fully glycosylated (100 kDa) NIS protein decreased during the 24 h treatment period, whereas partially glycosylated NIS fractions remained unaltered (Fig. 4C). Notice that endogenous calnexin expression was found to be more or less equal in all cell types, indicating a possible differential association/dissociation in the clonal cells (Fig. 4D).

N-linked glycosylation modulates plasma membrane localization of NIS

Taking clues from the data generated above, we saw that the different sub-cellular localization of NIS is a consequence of different cellular trafficking in breast cancer cells. Additionally, the human NIS protein has three putative N-glycosylation sites at amino acid positions 225, 485 and 497 (Levy et al., 1997). Therefore, we further questioned whether PTM, like N-linked glycosylation, is directly involved in NIS localization among the clonal cell variants. The cl31 cells, which represent membranous NIS were exposed to various glycosylation inhibitors, thereby interfering with different steps of N-linked glycosylation, as depicted in Fig. 5A. Inhibitors chosen were deoxymannojirimycin (DMM), swainsonine and tunicamycin, inhibiting various intermediate stages during the N-linked glycosylation process. Tunicamycin inhibits the first step of N-linked glycosylation, i.e. the addition of core oligosaccharide to nascent polypeptide. DMM is an inhibitor of class 1 alpha1, 2 mannosidase. Swainsonine is an inhibitor of

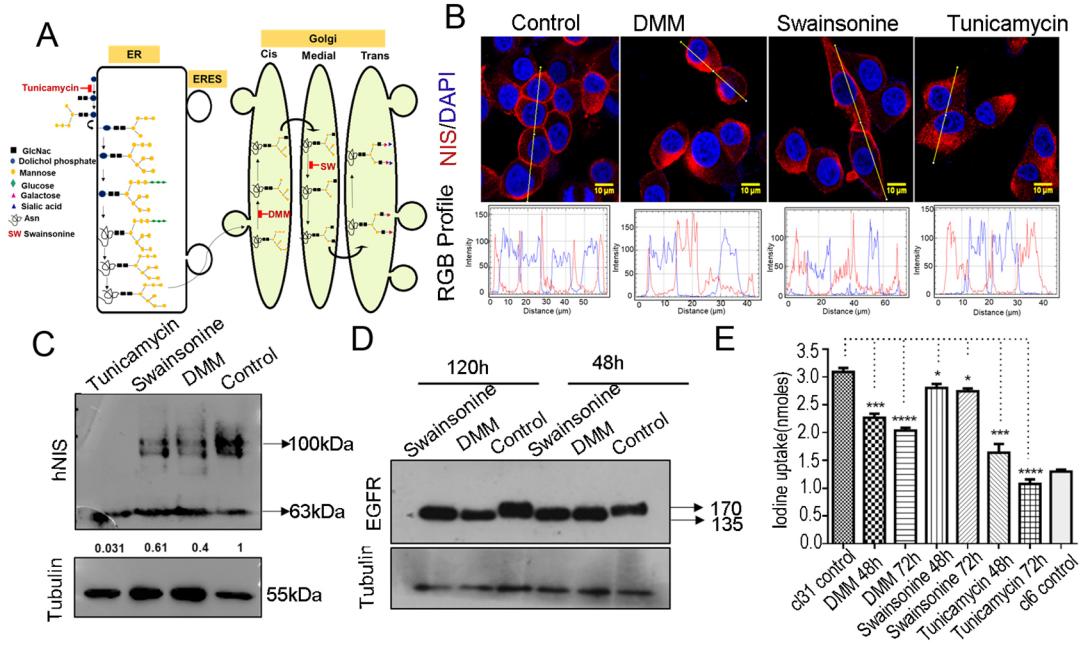

Fig. 5. Inhibition of N-linked glycosylation perturbs translocation of NIS to the plasma membrane. (A) Cartoon detailing glycan processing steps of a protein as it uses the secretory pathway, as well as the site of action of the inhibitors of N-linked glycosylation used in this research. (B) IF images showing treatment effect with step-specific glycosylation inhibitors DMM, tunicamycin and swainsonine at 48 h. The RGB histogram plotted below suggests incremental cytoplasmic staining of NIS in DMM- or tunicamycin-treated cells. Nucleus cross-staining was done using DAPI (blue). (C) Western blot showing a profound decrease in the mature glycosylated form of NIS (100 kDa) after 48 h of treatment with DMM, tunicamycin or swainsonine. Tubulin was used as an endogenous loading control. (D) Western blot showing the effect of N-linked glycosylation inhibitors on another endogenous protein EGFR in cl31 cells. (E) Effect of inhibition of NIS function measured by non-radioactive uptake of iodine. Cells that express NIS in their membrane and were treated with glycosylation inhibitors show a significant decrease in their iodine uptake ability. *P<0.05; ***P<0.001; ****P<0.0001.

Journal of Cell Science (2019) 132, jcs232058. doi:10.1242/jcs.232058

Golgi mannosidase 2. They were tested for their cytotoxicity in baseline MCF-7 cells, at selected concentrations below their half maximal inhibitory concentration (IC50) (Fig. S4A–C). IF of NIS was done in cl31 and cl6 cells after treating cells with inhibitors for 48 h. The cl31 cells treated with DMM or tunicamycin showed substantial loss of membrane-localized NIS, whereas swainsonine-treated cells showed only partial loss of membrane-localized NIS (Fig. 5B). As expected, treatment of cytoplasmic clone (cl6) with these inhibitors did not have any impact on NIS localization, as shown by RGB plot, clearly suggesting cytoplasmic staining of NIS before and after treatment with inhibitor (Fig. S4A). Swainsonine treatment of cl31 cells for a prolonged period of 120 h caused a substantial localization shift for NIS (Fig. S4B). The effect of these glycan inhibitors on NIS were further verified by western blotting. The apparent loss of the fully glycosylated NIS protein (100 kDa) in DMM- and tunicamycin-treated samples further supports the IF observations (Fig. 5C). To verify the effect of glycosylation inhibitors on other endogenous N-linked glycoproteins present in the cell, immunoblotting of EGFR shows a shift to non-glycosylated EGFR (~135 kDa) from the 170 kDa mature form of EGFR that is present in untreated control, indicating a global de-glycosylation effect in inhibitor-treated cells (Fig. 5D). To further support the effect of these inhibitors on NIS function, cl31 cells (membranous NIS) treated with DMM, swainsonine or tunicamycin for 48 or 72 h showed a significant reduction of iodine uptake compared to untreated cl31 cells (P<0.05). Additionally, the result also revealed that tunicamycin-treated cl31 and cl6 cells (membranous and cytoplasmic NIS, respectively) had equivalent iodine uptake ability, clearly indicating a loss of NIS function in response to interference of glycosylation (Fig. 5E).

Differential expression of several glycosylation genes constitute the difference in subcellular localization of NIS across the cell models

Now, knowing whether N-linked glycosylation is, indeed, an important player in modulating subcellular localization of NIS, we further investigated regulatory genes involved in the process. Total mRNA extracted from baseline MCF-7 cells and membranous or cytoplasmic NIS (hereafter referred to membranous or cytoplasmic NIS-expressing cells) were used for analysis on the RT-PCR profiler array platform (Fig. 6A). The heat map generated using the relative expression values of a set of 84 human genes involve in the cellular glycosylation process of the respective cells was analyzed. Interestingly, the data evidently showed that a specific set of 32 genes was upregulated in membrane clones, but downregulated in both cytoplasm clones and baseline MCF-7 cells. By further analyzing the data using ClustVis software, sample clustering was done, which showed that MCF-7 and cytoplasm clones, indeed, clustered together and classify distinctly than the membrane-expressing clones.

On the basis of the previous data, we found that the mannose-specific inhibitor DMM causes a reversal in the phenotype of cl31 cells. The array data further confirmed this observation, showing that mannosidase genes, such as *MAN1A1*, *MAN1B1*, *MAN2A1* and *MAN2A2*, indeed, show remarkable upregulation in membrane-expressing NIS clones compared with their counterparts that express NIS in the cytoplasm (Fig. 6B). Mannosyltransferase genes, i.e. *MGAT4B* or *MGAT5*, also show upregulation in membrane clones,

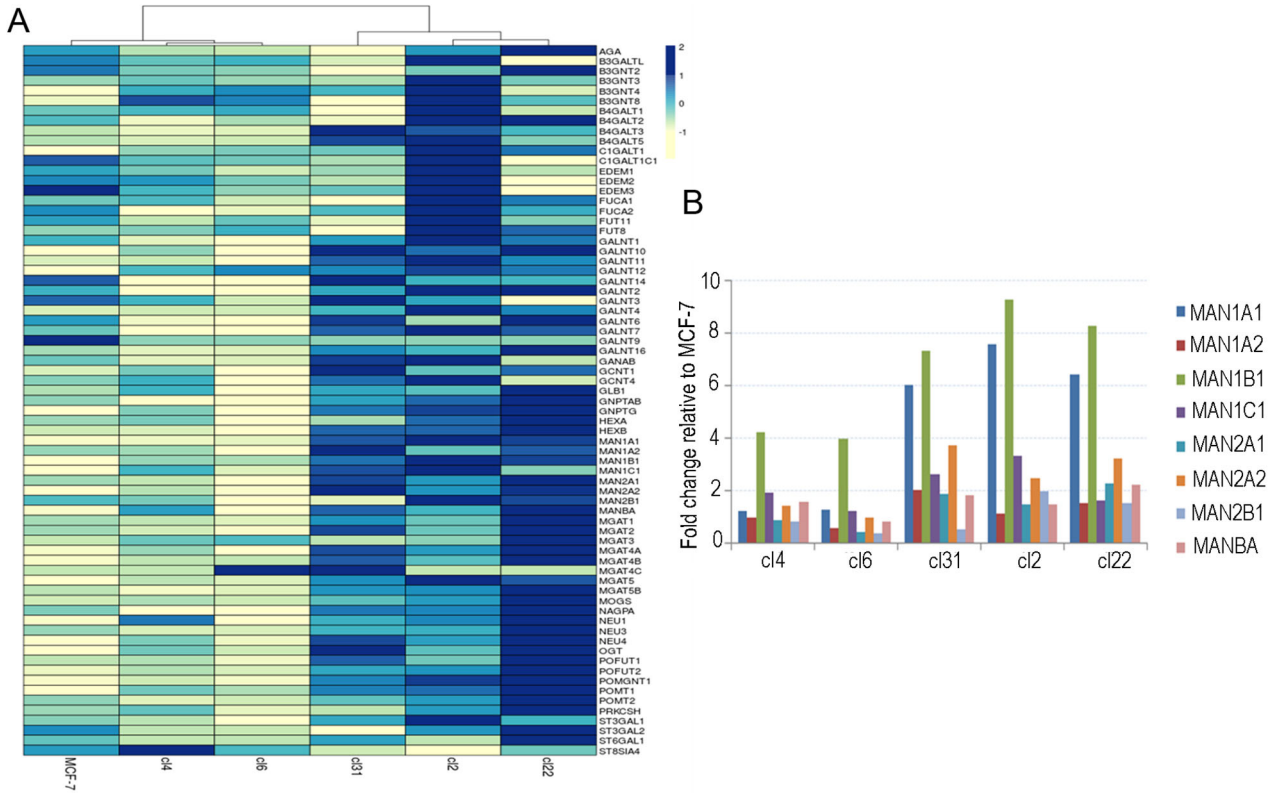

Fig. 6. Expression of glycosylation-regulating genes distinctively varies in clonal cells with different NIS localization. (A) Glycosylation RT-PCR array data show clear differences in the expression of glycosylation-regulating genes when comparing baseline MCF-7 cells, clonal cells expressing membranous NIS (cl31, cl22 and cl2) and clonal cells expressing cytoplasmic NIS (cl6, cl4). Clustering analysis by using the ClustVis software also shows distinct clusters that separate baseline cells and clonal cells expressing cytoplasmic NIS from clonal cells expressing membranous NIS. (B) Bar graph showing expression levels of different mannosidases in clonal cells.

Journal of Cell Science (2019) 132, jcs232058. doi:10.1242/jcs.232058

whereas MGAT4C shows downregulation in two out of three membrane clones (Fig. S6A). Among other genes *ST6GAL1* and *NEU4* should be noticed, as they are upregulated in the membrane clones (Fig. S6B,C).

Cellular mannosidase activity is a crucial determinant for membrane-specific localization of NIS

As revealed from the glycosylation gene array, membrane clones show higher expression of mannosidase genes such as *MAN1B1*, *MAN1A1* and *MAN2A1*. To validate the functional impact of these three mannosidases on NIS localization or function, we performed RNAi for endogenous gene knockdown in cl31 cells. Transcript analysis for each gene product after treatment with siRNA shows a 60–80% drop in relative mRNA expression (Fig. 7A). NIS expression was also verified by immunoblotting, where the fully glycosylated 100 kDa NIS band was considered as the main comparator among the samples (Fig. 7C). Immunoblot results show that knockdown of individual mannosidases reduced the 100 kDa NIS band, and was further reduced in response to dual knockdown of *MAN1B1*+*MAN1A1*, *MAN1A1*+*MAN2A1* or *MAN1B1*+*MAN2A1* as well as knockdown of all three candidates together. Our data convincingly point towards MAN1B1 as a central role player, impacting NIS glycosylation in this cell type because NIS sub-cellular localization by IF staining revealed that knockdown of *MAN1B1*, *MAN1A1* or *MAN2A1* disrupts NIS localization on cell surface, the most-prominent one being *MAN1B1*, where treated cells show major spreads of stained NIS in the cytoplasm (Fig. 7B). Further, the effect of mannosidase knockdown on NIS function was verified showing that treatment with siRNA against *MAN1B1*, *MAN1A1* or *MAN2A1* significantly ($P<0.005$) reduced cellular iodine uptake capacity when compared to untreated cells (Fig. 7D). As these mannosidase enzymes have a global effect on a number of glycoproteins, we also tested another endogenous protein, HER3, as control. We observed that, by knocking down these mannosidase genes alone, no prominent change in the HER3 localization occurred on the plasma membrane. However, by combining the three mannosidases, a significant reduction in HER3 protein expression on plasma membrane location was observed (Fig. 7E). Additionally, since our results revealed a role for the mannosidase class of enzymes regarding the sub-cellular localization of NIS, we tested for the presence of mannose on the NIS molecule. NIS was pulled down by immunoprecipitation (IP) from total cell lysates of cl31, cl6 and MCF-7 cells, and further western blotting was performed (Fig. S7A). As the data suggested, NIS obtained from cl31 cells showed the highest level of the 100 kDa fraction, i.e. NIS bound to mannose. Further, by probing with concavalin A (conA), the NIS IP fraction in cl31 was revealed to be the one with highest mannose glycosylation (Fig. 7F). Interestingly, as the mannose-positive band appeared at 100 kDa, matured NIS is a mannose-rich glycoprotein.

DISCUSSION

The unique potential of using NIS to mediate targeted radio-iodine ablation in breast cancer is severely impeded, as this aberrant and

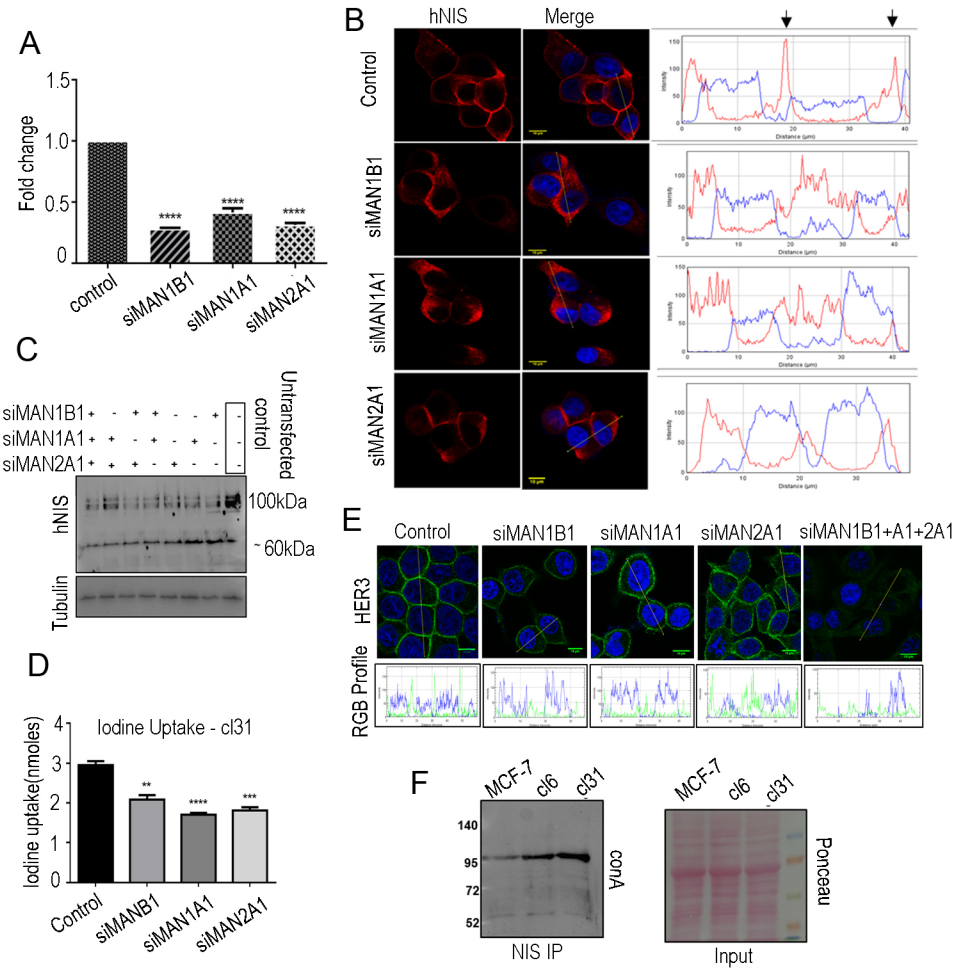

Fig. 7. Mannosidases are responsible for impaired trafficking of NIS in breast cancer. (A) Bar graph showing the knockdown effect of *MAN1B1*, *MAN1A1* and *MAN2A1* mRNAs after using siRNAs in cl31 cells. ****$P<0.0001$. (B) IF images and RGB histogram plots showing that MAN1B1, MAN1A1 and MAN2A1 knockdown effectively perturbs localization of NIS (red) to the cytoplasm. Cross-staining of the nucleus was done with DAPI (blue). Scale bars: 10 µm. (C) Western blot showing the effect knockdown of MAN1B1, MAN1A1, MAN2A1 and their respective combinations has on NIS glycosylation. The 100 kDa band corresponds to completely glycosylated NIS; partly glycosylated NIS has a molecular mass of 60 kDa. Tubulin was used as an endogenous loading control. (D) Bar graph showing significantly reduced function (**$P<0.01$; ***$P<0.001$; ****$P<0.0001$) observed for NIS-mediated iodine uptake in cl31 cells in response to siRNA treatment of individual mannosidases. Error bars represent +s.e.m. (E) IF images and RGB histogram plots showing MAN1B1, MAN1A1 and MAN2A1 triple knockdown effectively perturbs localization of HER3 (green) to the cytoplasm. Cross-staining of the nucleus was done with DAPI (blue). Scale bars: 10 µm. (F) Western blotting using lectin (conA) to detect mannose in purified NIS fractions, showing that the NIS fraction from cl31 cells has highest amount of mannose, which appears at the position of the mature 100-kDa form of NIS. Ponceau staining of input used to confirm equal loading.

Journal of Cell Science (2019) 132, jcs232058. doi:10.1242/jcs.232058

endogenously overexpressed pump protein primarily stays in the cytoplasm (Micali et al., 2014). Elucidation of the factors that regulate NIS localization in non-thyroidal cancer cells revealed information on defective glycosylation as the root cause of NIS malfunction (Chung et al., 2015; Levy et al., 1997). This study brings new evidence in this direction and identifies key molecules involved in the deregulated glycosylation that is responsible for impaired NIS function in breast cancer cells.

The cell model utilized in this study is unique but, rather, an offshoot from another interesting observation in which – by expressing the AttB-CAG-driven bi-cistronic NIS-IRES-TurboFP.Fluc2 transgene in the MCF-7 breast adenocarcinoma cell line – two clearly distinguishable phenotypes were obtained. A few clones with variable amount of NIS protein on the plasma membrane (cl30, cl31, cl32, cl34, cl22, cl2.) was, ideally, what we wanted to find. However, a majority of others clones showed cytoplasmic expression of NIS (cl4, cl6 etc.), allowing us to investigate the basis of defective NIS function. The difference in the NIS localization pattern is striking and can be explained by the purview of current understandings regarding clonal heterogeneity, especially when the baseline cell is a clonal cancer cell. Previous reports have explained that different clones derived from the same cell line could possess different properties (Hastings and Franks, 1983). Karyotypic differences across the derived clonal population provide further evidence of cancer cell heterogeneity that lies within the cell population itself. But, importantly, retention of respective features over a number of passages is very reassuring, supporting their true clonal nature. The difference in iodine pump function also brings further support to the genuine nature of the observed variation in NIS localization.

Thereafter, we enquired whether this difference is due to PTM, i.e. N-linked glycosylation, regulating membrane protein translocation. A past study has shown that treatment with tunicamycin can reverse NIS location (Chung et al., 2015). Tunicamycin inhibits the first step of glycosylation, during which attachment of GalNc to the dolichol phosphate anchor occurs (Wojtowicz et al., 2012). Our current study also describes a decrease in membrane-localized NIS upon treatment with this inhibitor. Additionally, the role of other steps of the glycan maturation process of NIS inside the cell are shown. In our study, we used DMM and swainsonine. DMM inhibits the activity of Golgi mannosidase 1, which is required for processing the 8-mannose form to the 5-mannose form, intermediates that are generated during the N-linked glycosylation in the Golgi, when mannose units are cleaved from the core glycan by enzymes, such as mannosidases. This event is important for trafficking of glycans in Golgi (Gross et al., 1986). DMM treatment of cl31 shows severe defects in the membrane localization of NIS within 48 h, such that they more resemble the cytoplasm clones. Swainsonine is a mannosidase II activity inhibitor that inhibits the late maturation process of N-glycans in the Golgi complex (Elbein et al., 1981); it shows a much delayed response (i.e. 120 h) in terms of altering membrane localization of NIS. These results indicate that the early steps of mannose modification are crucial in determining the sub-cellular fate of NIS. Results obtained from trafficking colocalization studies further confirmed that, in the clonal membrane type (cl31), NIS is present in the ER and, as the Golgi restores after treatment with BFA, can enter the Golgi. However, in the clonal cytoplasm type (cl6) and in baseline MCF-7 cells, the ER-to-Golgi transit is restrained after Golgi restoration. In fact, as opposed to the membrane clone, cytoplasm cells show accumulation of NIS in ER/ER exit sites, even when Golgi restoration is complete. The proteins that are incapable of folding appropriately, undergo ER quality control through a series of calnexin/calreticulin cycles, where they are allowed to gain their correct confirmation (Caramelo and Parodi, 2015). Our results further showed that the association of NIS with calnexin is significantly higher ($P<0.05$) in MCF-7 and cl6 cells compared with cl31 cells. Those proteins that fail to fold in spite of this quality control come to the cytoplasm through ER translocation channels and are degraded by proteasomes (Ahner and Brodsky, 2004). Cytosolic localization of NIS in case of MCF-7 and cl6 cells might, perhaps, face this fate (not verified). Together, all these results indicate a very important aspect on NIS protein localization, i.e. NIS undergoes initial glycan processing in the ER and, if when this process is compromised, breast cancer cells show cytoplasmic accumulation and NIS dysfunction.

Thereafter, we focus on identifying key glycosylation genes that are differentially regulated in the clonal cell variants and baseline MCF-7. Based on the expression pattern obtained by analyzing a set of 84 genes present in the transcript array, baseline MCF-7 and clonal cells with cytoplasmic NIS localization do cluster together. However, clones that express membranous NIS cluster separately, showing differential upregulation of genes primarily belonging to mannosidases, mannosyltransferases, sialidases and neuramindases. These results sufficiently indicate that altered expression of certain important genes related to glycosylation-processing function in the clonal variants is widely different, thus, bringing out the difference in NIS localization and function. We further focus on investigating the role of mannosidases, focusing on MAN1B1, MAN1A1 and MAN2A1 highlighted in the Glycosylation RT profiler array data. These showed upregulation in cl31 as compared to cl6. MAN1B1 and MAN1A1 are class 1 α-mannosidases that help to cleave the terminal mannose moieties from core glycan. MAN1B1 acts on the β-branch of mannose. Both MAN1A1 and MAN1B1 are localized in the ER, whereas MAN2A1 is localized in the Golgi, which helps in the final maturation of glycoprotein. By knocking down these mannosidases individually or in combination caused substantial reduction of NIS expression at cell surface of the membrane clones and, thus, impacted the cellular iodine uptake ability. In view of the known importance of initial mannose modifications for NIS maturation, our results imply that the three mannosidases have an important role in trafficking NIS to the cell membrane. When sufficient glycosylation processing enzymes are present N-glycan processing takes place effectively, leading to correct folding of NIS. This, in turn, boosts successful trafficking of NIS from ER to Golgi and finally to the cell membrane.

In summary, our results show for the first time that inadequate mannose processing by mannosidase enzymes is deeply involved in sugar modification at the ER site in breast cancer cells (Fig. 8). Since cellular defects in glycosylation processes are responsible for mislocalization of NIS in breast cancer cells, the molecular targets validated here actually impact on impaired NIS function in breast cancer. The second messenger cyclic AMP (cAMP), mediates the first step of N-linked glycosylation, improving levels of dolichol pyrophosphate oligosaccharide (Konrad and Merz, 1994). Thus, pre-treatment with cAMP can also enhance membrane localization of NIS. Further, validation of additional regulators identified here, such as sialidases and neuramindases, might help our understanding of how N-glycosylation impacts on NIS localization in breast cancer cells and, thus, might provide a scope of furthering any of those molecular targets for the clinical use of this pump protein as a therapeutic candidate.

MATERIALS AND METHODS

Materials

D-luciferin was procured from Biosynth chemistry and biology (L-8220), brefeldin A (BFA) from Sigma, (B7651), Deoxymannojirimycine (DMM) and tunicamycin from Sigma (D9305 and T7765, respectively),

Journal of Cell Science (2019) 132, jcs232058. doi:10.1242/jcs.232058

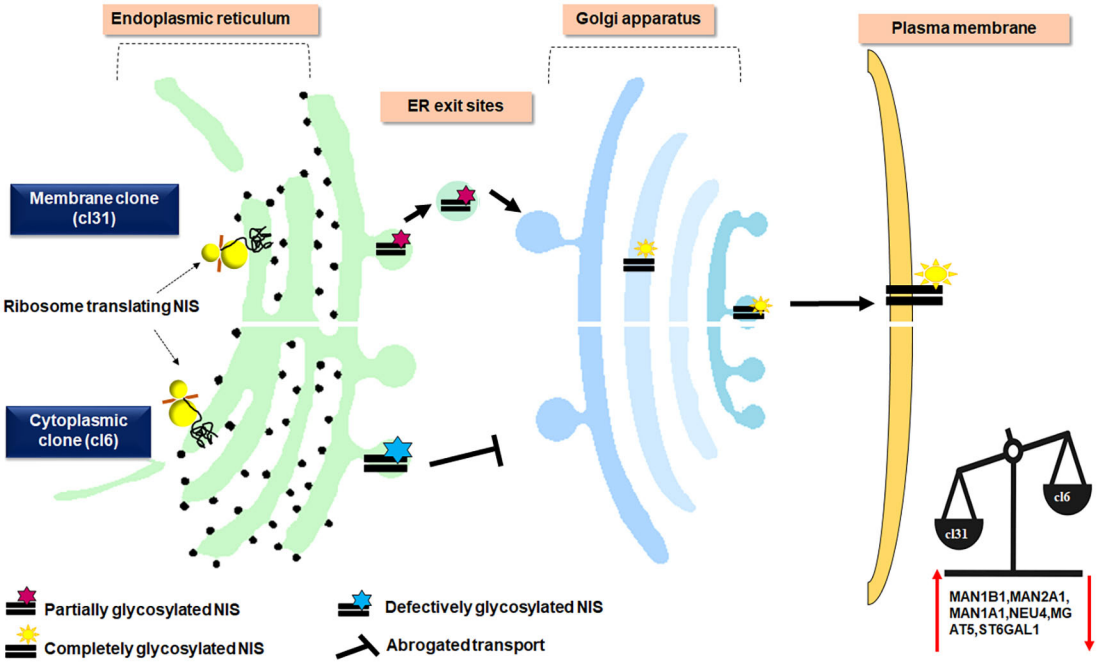

Fig. 8. Schematic diagram showing important aspects of mannose glycosylation and trafficking defects found for NIS protein in two populations of MCF-7 cells. In the case of cl31, human NIS undergoes stepwise post-translation events in cellular organelles, such as the ER and the Golgi complex, which enables NIS to localize to the cell membrane. This is in contrast to NIS in cl6, where it faces incomplete glycosylation owing to reduced levels of glycosylation enzymes, such as MAN1B1 and MAN2A1. In this case NIS is unable to pass through ER exit sites.

Glycosylation RT-PCR array was from Qiagen (PAH546Z), Silencer select siRNA smartpools from Life Technologies (4392426), CellLight ER-GFP, Bacmam from Thermo Fisher scientific (C10590), Luciferase Assay system from Promega (E4030). We used EGFR primary antibody (Cell Signaling Technology, 4267S, 1:100), HER3 monoclonal antibody (Cell Signaling Technology, 12708S, 1:100), human sodium iodide symporter antibody (Thermo Scientific (MA5-12308, 1:50), α-tubulin primary antibody (Sigma, T9026), calnexin antibody (Cell Signaling Technology, C5C9, 1:50), anti-mouse HRP secondary antibody (Abcam, ab6728), goat anti-rabbit HRP antibody (Thermo Scientific, 31460), goat anti-rabbit DyLight 488 secondary antibody (Thermo Fisher Scientific, 35552), goat anti-mouse DyLight 633 secondary antibody (Thermo Fisher Scientific, 35512), Biotynylated conA lectin (Sigma, C2272), avidin-peroxidase (Sigma, A3151).

Generation of stable NIS-overexpressing cell lines

The NIS-IRES-FL2.turboFP bi-cistronic DNA cassette was sub-cloned in attb-CAG phage integrase mammalian expression vector (Groth et al., 2000). Cells of the MCF-7 breast cancer cell line were transfected with attb-CAG NIS-IRES-FL2.turboFP plasmid DNA using Lipofectamine 2000 reagent. After 48 h cells were kept in RPMI-1640 with 10% FBS (Gibco) supplemented with 600 µg/ml G418 antibiotic. Once colonies formed, cells were transferred to 96-well plates and propagated further. Positive clones were picked up after luciferase assay using LAR II substrate. Cells were constantly maintained under G418 selection until freezing cells in liquid N_2. Expression of NIS was verified by IF.

Luciferase reporter assay

Luciferase assays were performed as per recommended standard protocol. Clonal cells from replica plates were lysed using cell lysis buffer and reporter activity was measured using a microplate reader (BMG Labtech) after adding LARII substrate to each well. The relative light units (RLUs) were normalized to the respective protein concentrations of the lysates.

Immunoblotting

Cells were lysed using RIPA buffer containing protease inhibitor cocktail. Equal amounts of protein from control and transfected/treated cells were separated by 7.5% SDS-PAGE and transferred onto a nitrocellulose membrane by using a semi-dry blotting apparatus. After blocking with 5% non-fat dry milk, membranes were probed with antibodies against human NIS, α-tubulin, EGFR and calnexin. The blots were then probed with HRP-conjugated secondary antibodies and developed using a Chemidoc system. Cells were treated with cyclohexamide (chx) at 40 µg/ml) at different time points. Lysates were then collected and analysed by immunoblotting.

Immunoprecipitation and lectin western blot

A standard IP protocol was followed with the following specifications: Cell lysates were prepared using RIPA lysis buffer and 250 µg of protein from each sample was used for IP. Sepharose G beads were blocked with 2% BSA and used for IP. RIPA buffer with low SDS (0.01%) was used as IP dilution buffer. NIS was pulled down with 2 µg primary antibody by incubating the bead antibody and lysates together overnight at 4°C under constant rotation. Following the IP, NIS was eluted from the immune-complex with urea buffer according to instructions provided in protocol for IP provided by Abcam. Biotynylated concavalin A (conA) lectin was used to probe the purified product of IP on nitrocellulose membrane at a concentration of 15 µg/ml in TBST for 1 h at RT. The blot was then probed with streptavidin HRP-conjugated secondary antibody at 1:30,000 dilution.

Immunofluorescence

For immunofluorescence (IF) studies, cells were fixed with 4% paraformaldehyde. Blocking was done using 2% BSA followed by overnight incubation with NIS, HER3 or calnexin antibodies at 4°C. The cells were then washed with PBS, incubated with anti-mouse or anti-rabbit Dylight 633 secondary antibody for 1 h. Fluorescence micrographs were captured by using a Carl Zeiss LSM 780 confocal microscope using a 63× objective with a numerical aperture of 1.3 and a pinhole restricted to 1 AU (1 AU=0.7 µm). The images for colocalization experiments were captured by sequential independent scanning of both channels to exclude cross-talks. The acquisition software used was Zen2012. To study the colocalization of NIS and different cell organelle markers, cells were transfected with GalNac T2-GFP and sec16B-GFP plasmids to, respectively, mark Golgi and ERES, and transduced for 48 h with CellLight™ ER-GFP bacculovirus that marks the ER through present KDEL sequences. Cells were then treated with brefeldin A

(BFA) (5 µg/ml) for 30 min to disrupt the Golgi, followed by a rescue period of 6 h and 12 h. RGB plot profiles were made using ImageJ software. Images were stacked to RGB mode and then the plots were measured under the graphics section in ImageJ. The plot shows the intensity of all points on the line of interest drawn on the image. Intensities are measured for all channels in that image, in our case red and blue. The RGB plot *x*-axis shows the distance in µm and the *y*-axis shows the intensity. Accumulation of proteins only at the surface of the cell, will give a sharp peak of red intensity at that site on the line of interest, whereas cytoplasmic staining gives a more-distributed pattern of red intensities.

Real-time PCR

After transfecting cl31 cells with 20 nM siRNA by using Lipofectamine RNAi max, for 48 h, RNA was extracted using an RNeasy kit. cDNAs were synthesized by using the first-strand cDNA synthesis kit. Sequences of duplex siRNA and PCR primers are in shown in Table S2. Quantitative real-time PCR (RT-PCR) was performed using SYBR Green probe mix on the 7900HT PCR cycler (Applied Biosystems). Triplicate samples were run for each sample. The comparative ΔΔCt method was used to calculate relative gene expression.

Iodine uptake assay

Iodine uptake was done using standardized non-radioactive assay method as described before (Kelkar et al., 2016).

Glycosylation RT-profiler PCR array

Glycosylation PCR arrays were carried out as per recommended protocol (Qiagen). RNA samples was isolated from various cell clones tested using an RNAeasy kit (Qiagen) and residual DNA was digested on the column with RNAse H, as provided in the kit. Quality of RNA was checked by using a denaturing RNA gel and cDNA was prepared using 1 µg of RNA per sample by using an AffinityScript cDNA synthesis kit (ThermoFisher). cDNA and SYBR Green were loaded together with the PCR mix in individual wells, which already contained the primer for the reaction. After RT-PCR was carried out using Quantstudio 12K flex, data were uploaded to DRYAD and analyzed using ClustVis software.

Statistics

All data are expressed as mean±s.e. Statistical significance was analysed by Student's *t*-test using GraphPad Prism 6 software (GraphPad Software, La Jolla, CA). Two-way ANOVA (Tukey's multiple comparison test) was used to analyze statistical significances of the overlap coefficient values obtained for NIS and EGFR with that of ER-, ERES- and Golgi-specific organelle markers at various time points. Overlap coefficient values were counted from an average of 40–45 cells per sample in various experiments done. *P* values of ≤ 0.05 were considered statistically significant and the confidence interval (CI) was set at 95%. Statistical analysis was done for a minimum of two independent biological repeats. ClustVis software was used for cluster analysis of gene expression profiler array datasets.

Competing interests

The authors declare no competing or financial interests.

Author contributions

Conceptualization: S.C., A.D.; Methodology: M.R., S.C., S.D., D.B., A.D.; Software: D.B.; Validation: M.R., S.C., R.K.; Formal analysis: M.R., S.C., D.B., A.D.; Investigation: M.R., S.C., S.D., R.K.; Resources: S.C., R.K., D.B., A.D.; Data curation: M.R., A.D.; Writing - original draft: M.R.; Writing - review & editing: S.C., S.D., D.B., A.D.; Visualization: A.D.; Supervision: A.D.; Project administration: A.D.; Funding acquisition: S.D., A.D.

Funding

For this research, A.D. was funded by a Dr Rajiv Kalraiya Memorial Research grant (DRKMR) and S.D. by a DST-WoS grant award (DST-WOSA: SR/WOS-A/LS-1112/2014).

Data availability

RT-PCR data are available from the Dryad Digital Repository (Rathod et al. 2019): https://doi.org/10.5061/dryad.r7sqv9s7f

Supplementary information

Supplementary information available online at
http://jcs.biologists.org/lookup/doi/10.1242/jcs.232058.supplemental

References

Aebi, M. (2013). N-linked protein glycosylation in the ER. *Biochim. Biophys. Acta* **1833**, 2430-2437. doi:10.1016/j.bbamcr.2013.04.001

Ahner, A. and Brodsky, J. L. (2004). Checkpoints in ER-associated degradation: excuse me, which way to the proteasome? *Trends Cell Biol.* **14**, 474-478. doi:10.1016/j.tcb.2004.07.013

Benyair, R., Ogen-Shtern, N. and Lederkremer, G. Z. (2015). Glycan regulation of ER-associated degradation through compartmentalization. *Semin. Cell Dev. Biol.* **41**, 99-109. doi:10.1016/j.semcdb.2014.11.006

Beyer, S. J., Jimenez, R. E., Shapiro, C. L., Cho, J. Y. and Jhiang, S. M. (2009). Do cell surface trafficking impairments account for variable cell surface sodium iodide symporter levels in breast cancer? *Breast Cancer Res. Treat.* **115**, 205-212. doi:10.1007/s10549-008-0059-5

Beyer, S., Lakshmanan, A., Liu, Y.-Y., Zhang, X., Wapnir, I., Smolenski, A. and Jhiang, S. (2011). KT5823 differentially modulates sodium iodide symporter expression, activity, and glycosylation between thyroid and breast cancer cells. *Endocrinology* **152**, 782-792. doi:10.1210/en.2010-0782

Caramelo, J. J. and Parodi, A. J. (2015). A sweet code for glycoprotein folding. *FEBS Lett.* **589**, 3379-3387. doi:10.1016/j.febslet.2015.07.021

Chatterjee, S., Malhotra, R., Varghese, F., Bukhari, A. B., Patil, A., Budrukkar, A., Parmar, V., Gupta, S. and De, A. (2013). Quantitative immunohistochemical analysis reveals association between sodium iodide symporter and estrogen receptor expression in breast cancer. *PLoS ONE* **8**, e54055. doi:10.1371/journal.pone.0054055

Chung, T., Youn, H., Yeom, C. J., Kang, K. W. and Chung, J.-K. (2015). Glycosylation of sodium/iodide symporter (NIS) regulates its membrane translocation and radioiodine uptake. *PLoS ONE* **10**, e0142984. doi:10.1371/journal.pone.0142984

Connerly, P. L., Esaki, M., Montegna, E. A., Strongin, D. E., Levi, S., Soderholm, J. and Glick, B. S. (2005). Sec16 is a determinant of transitional ER organization. *Curr. Biol.* **15**, 1439-1447. doi:10.1016/j.cub.2005.06.065

Dutta, S. and De, A. (2015). Cancer gene therapy: Prospects of using human sodium iodide symporter gene in non-thyroidal cancer. *Biomed. Res. J.* **2**, 198-219. doi:10.4103/2349-3666.240655

Elbein, A. D., Solf, R., Dorling, P. R. and Vosbeck, K. (1981). Swainsonine: an inhibitor of glycoprotein processing. *Proc. Natl. Acad. Sci. USA* **78**, 7393-7397. doi:10.1073/pnas.78.12.7393

Gross, V., Tran-Thi, T. A., Schwarz, R. T., Elbein, A. D., Decker, K. and Heinrich, P. C. (1986). Different effects of the glucosidase inhibitors 1-deoxynojirimycin, N-methyl-1-deoxynojirimycin and castanospermine on the glycosylation of rat alpha 1-proteinase inhibitor and alpha 1-acid glycoprotein. *Biochem. J.* **236**, 853-860. doi:10.1042/bj2360853

Groth, A. C., Olivares, E. C., Thyagarajan, B. and Calos, M. P. (2000). A phage integrase directs efficient site-specific integration in human cells. *Proc. Natl. Acad. Sci. USA* **97**, 5995-6000. doi:10.1073/pnas.090527097

Hastings, R. J. and Franks, L. M. (1983). Cellular heterogeneity in a tissue culture cell line derived from a human bladder carcinoma. *Br. J. Cancer* **47**, 233-244. doi:10.1038/bjc.1983.31

Jung, K.-H., Paik, J.-Y., Ko, B.-H. and Lee, K.-H. (2008). Mitogen-activated protein kinase signaling enhances sodium iodide symporter function and efficacy of radioiodide therapy in nonthyroidal cancer cells. *J. Nuclear Med.* **49**, 1966-1972. doi:10.2967/jnumed.108.055764

Kelkar, M. G., Senthilkumar, K., Jadhav, S., Gupta, S., Ahn, B.-C. and De, A. (2016). Enhancement of human sodium iodide symporter gene therapy for breast cancer by HDAC inhibitor mediated transcriptional modulation. *Sci. Rep.* **6**, 19341. doi:10.1038/srep19341

Knostman, K. A. B., McCubrey, J. A., Morrison, C. D., Zhang, Z., Capen, C. C. and Jhiang, S. M. (2007). PI3K activation is associated with intracellular sodium/iodide symporter protein expression in breast cancer. *BMC Cancer* **7**, 137. doi:10.1186/1471-2407-7-137

Konrad, M. and Merz, W. E. (1994). Regulation of N-glycosylation. Long term effect of cyclic AMP mediates enhanced synthesis of the dolichol pyrophosphate core oligosaccharide. *J. Biol. Chem.* **269**, 8659-8666.

Levy, O., Dai, G., Riedel, C., Ginter, C. S., Paul, E. M., Lebowitz, A. N. and Carrasco, N. (1997). Characterization of the thyroid Na+/I- symporter with an anti-COOH terminus antibody. *Proc. Natl. Acad. Sci. USA* **94**, 5568-5573. doi:10.1073/pnas.94.11.5568

Levy, O., De la Vieja, A., Ginter, C. S., Riedel, C., Dai, G. and Carrasco, N. (1998). N-linked glycosylation of the thyroid Na+/I- symporter (NIS). Implications for its secondary structure model. *J. Biol. Chem.* **273**, 22657-22663. doi:10.1074/jbc.273.35.22657

Love, H. D., Lin, C.-C., Short, C. S. and Ostermann, J. (1998). Isolation of functional Golgi-derived vesicles with a possible role in retrograde transport. *J. Cell Biol.* **140**, 541-551. doi:10.1083/jcb.140.3.541

Micali, S., Bulotta, S., Puppin, C., Territo, A., Navarra, M., Bianchi, G., Damante, G., Filetti, S. and Russo, D. (2014). Sodium iodide symporter (NIS) in extrathyroidal malignancies: focus on breast and urological cancer. *BMC Cancer* **14**, 303. doi:10.1186/1471-2407-14-303

Moon, D. H., Lee, S. J., Park, K. Y., Park, K. K., Ahn, S. H., Pai, M. S., Chang, H., Lee, H. K. and Ahn, I.-M. (2001). Correlation between 99mTc-pertechnetate uptakes and expressions of human sodium iodide symporter gene in breast tumor tissues. *Nucl. Med. Biol.* **28**, 829-834. doi:10.1016/S0969-8051(01) 00243-8

Munro, S. and Pelham, H. R. B. (1987). A C-terminal signal prevents secretion of luminal ER proteins. *Cell* **48**, 899-907. doi:10.1016/0092-8674(87)90086-9

Paroder, V., Nicola, J. P., Ginter, C. S. and Carrasco, N. (2013). The iodide-transport-defect-causing mutation R124H: a delta-amino group at position 124 is critical for maturation and trafficking of the Na+/I– symporter. *J. Cell Sci.* **126**, 3305-3313. doi:10.1242/jcs.120246

Parodi, A. J. (2000). Role of N-oligosaccharide endoplasmic reticulum processing reactions in glycoprotein folding and degradation. *Biochem. J.* **348**, 1-13. doi:10.1042/bj3480001

Renier, C., Yao, C., Goris, M., Ghosh, M., Katznelson, L., Nowles, K., Gambhir, S. S. and Wapnir, I. (2009). Endogenous NIS expression in triple-negative breast cancers. *Ann. Surg. Oncol.* **16**, 962-968. doi:10.1245/s10434-008-0280-9

Riedel, C., Dohán, O., De la Vieja, A., Ginter, C. S. and Carrasco, N. (2001a). Journey of the iodide transporter NIS: from its molecular identification to its clinical role in cancer. *Trends Biochem. Sci.* **26**, 490-496. doi:10.1016/S0968-0004(01) 01904-1

Riedel, C., Levy, O. and Carrasco, N. (2001b). Post-transcriptional regulation of the sodium/iodide symporter by thyrotropin. *J. Biol. Chem.* **276**, 21458-21463. doi:10.1074/jbc.M100561200

Ryan, J., Curran, C. E., Hennessy, E., Newell, J., Morris, J. C., Kerin, M. J. and Dwyer, R. M. (2011). The sodium iodide symporter (NIS) and potential regulators in normal, benign and malignant human breast tissue. *PloS one* **6**, e16023. doi:10.1371/journal.pone.0016023

Tazebay, U. H., Wapnir, I. L., Levy, O., Dohan, O., Zuckier, L. S., Zhao, Q. H., Deng, H. F., Amenta, P. S., Fineberg, S., Pestell, R. G. et al. (2000). The mammary gland iodide transporter is expressed during lactation and in breast cancer. *Nat. Med.* **6**, 871-878. doi:10.1038/78630

Wapnir, I. L., van de Rijn, M., Nowels, K., Amenta, P. S., Walton, K., Montgomery, K., Greco, R. S., Dohán, O. and Carrasco, N. (2003). Immunohistochemical profile of the sodium/iodide symporter in thyroid, breast, and other carcinomas using high density tissue microarrays and conventional sections. *J. Clin. Endocrinol. Metab.* **88**, 1880-1888. doi:10.1210/jc.2002-021544

Weng, T.-Y., Chiu, W.-T., Liu, H.-S., Cheng, H.-C., Shen, M.-R., Mount, D. B. and Chou, C.-Y. (2013). Glycosylation regulates the function and membrane localization of KCC4. *Biochim. Biophys. Acta* **1833**, 1133-1146. doi:10.1016/j.bbamcr.2013.01.018

Wojtowicz, K., Szaflarski, W., Januchowski, R., Zawierucha, P., Nowicki, M. and Zabel, M. (2012). Inhibitors of N-glycosylation as a potential tool for analysis of the mechanism of action and cellular localisation of glycoprotein P. *Acta Biochim. Pol.* **59**, 445-450. doi:10.18388/abp.2012_2076

Zhou, F., Xu, W., Hong, M., Pan, Z., Sinko, P. J., Ma, J. and You, G. (2005). The role of N-linked glycosylation in protein folding, membrane targeting, and substrate binding of human organic anion transporter hOAT4. *Mol. Pharmacol.* **67**, 868-876. doi:10.1124/mol.104.007583

S1A

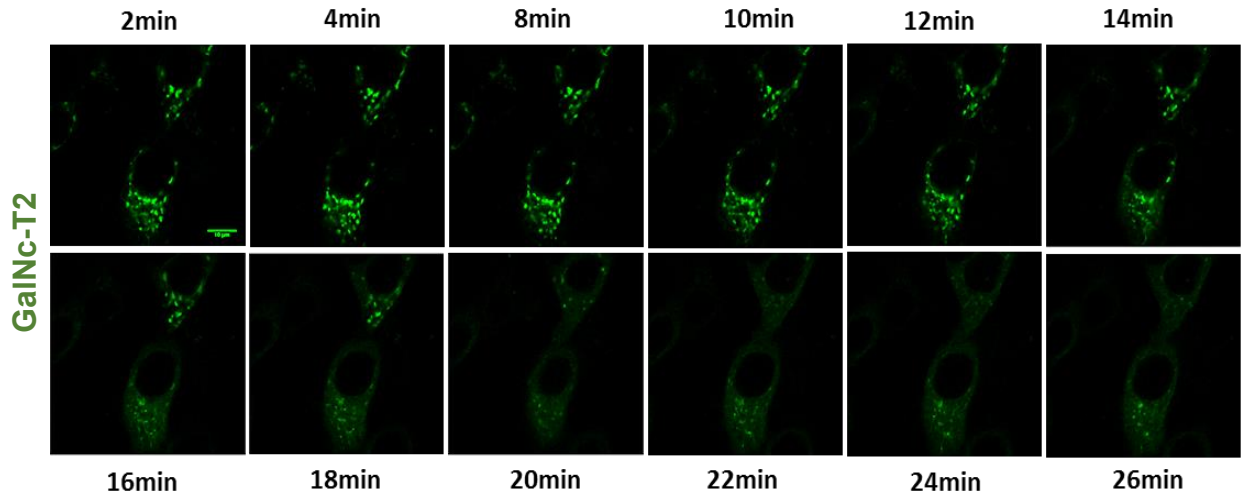

S1B

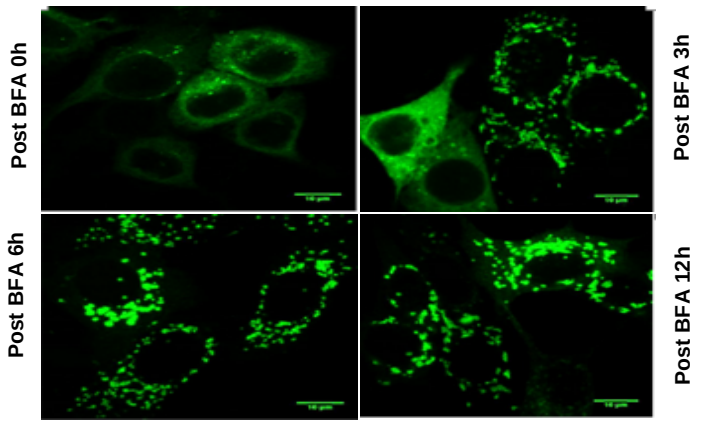

Figure S1: Effect of Brefeldin A (BFA) on Golgi deformation/reformation kinetics.

S1A. Live cell imaging of GalNac-T2-GFP (green) reporter at different time intervals, post BFA treatment, in MCF-7 cells (Live cell movie split into images). **S2B.** Golgi rescue kinetics, post BFA withdrawal in MCF-7 cells, as seen by GalNac-T2-GFP (green) reporter. The scale bar represents 10µm.

S2A

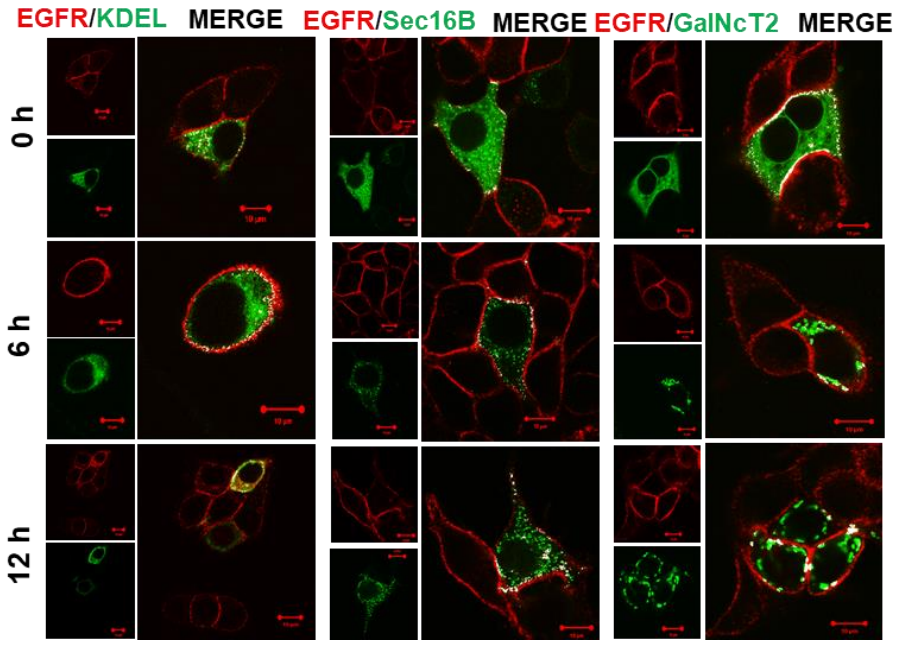

S2B

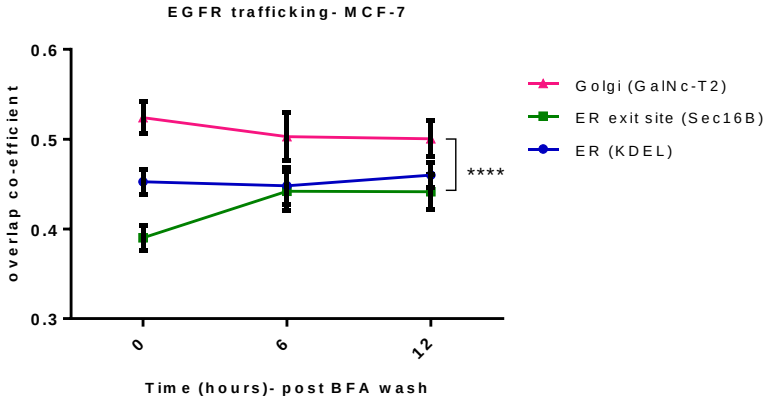

S2C

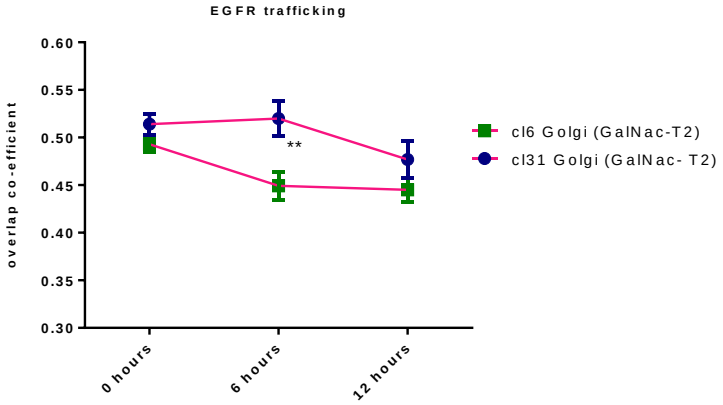

Figure S2: The trafficking of EGFR through Golgi across the clonal model systems. S2A. Co-localization of EGFR (red) with GalNac T2 (green) respectively in MCF-7 cells. All images represent a single plane. White spots are the points of co- localization between the two channels. The scale bar represents 10µm. **S2B.** Chart showing overlap co-efficients values obtained for EGFR with GalNac T2, Sec16B, and KDEL in MCF-7 cells. The middle best plane was used for quantification. Error bars indicate SEM. **S2C.** Chart showing overlap co-efficients values obtained for EGFR with GalNac T2 in cl31 and cl6 cells. The middle best plane was used for quantification. Error bars indicate SEM

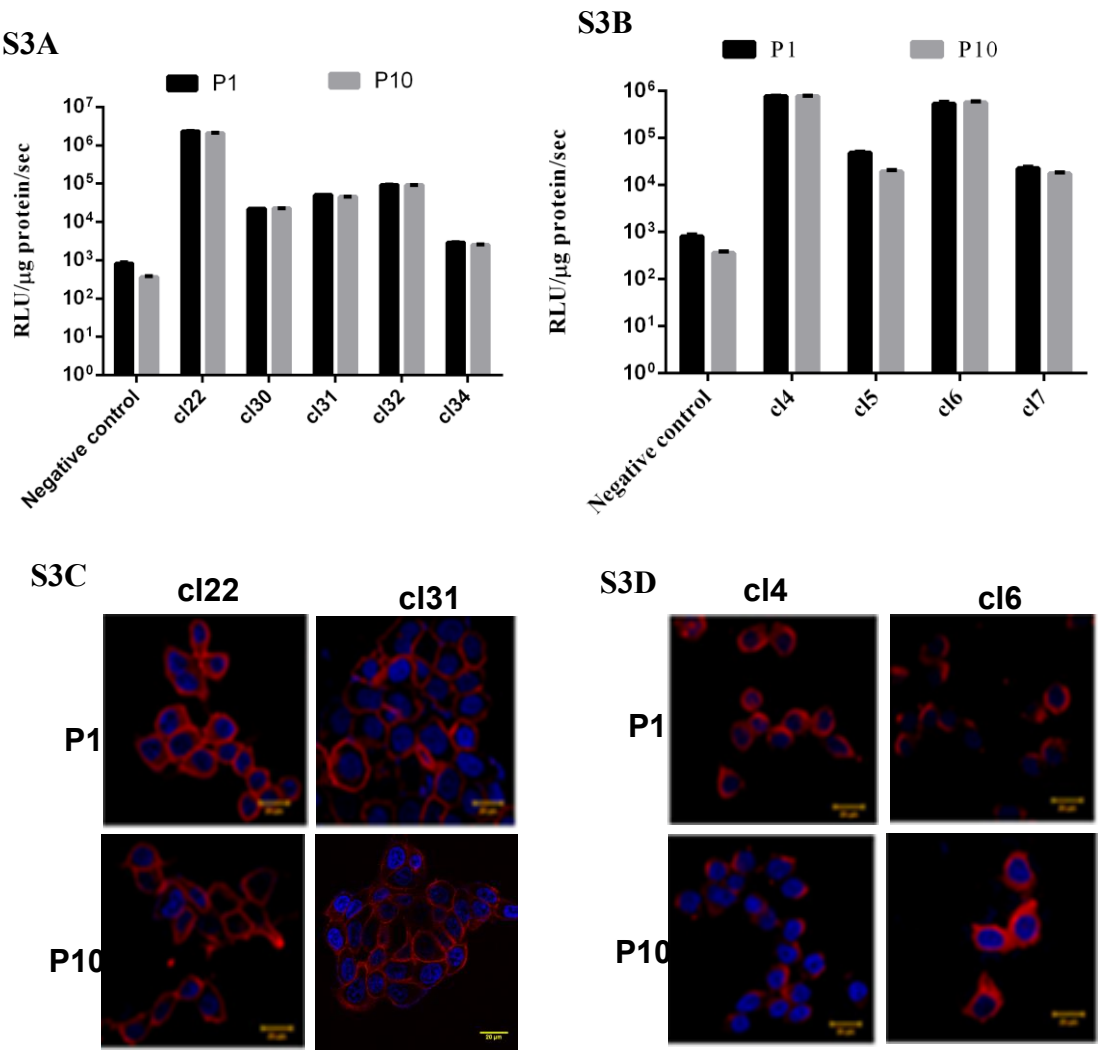

Figure S3: Stable expression of NIS in the clonal cell models is maintained over long passages. S3A-B. Luciferase assay showing relative light output normalized to protein concentration of Fl2 activity in membrane and cytoplasmic NIS overexpressing clones across passage 1 and passage 10 **S3C-D.** IF images showing the localization of NIS in membrane clones and cytoplasmic clones across passage 1 to 10. NIS stained with Dylight 633 secondary antibody (red) and nucleus staining by DAPI (blue). The scale bar represents 20µm.

S4A

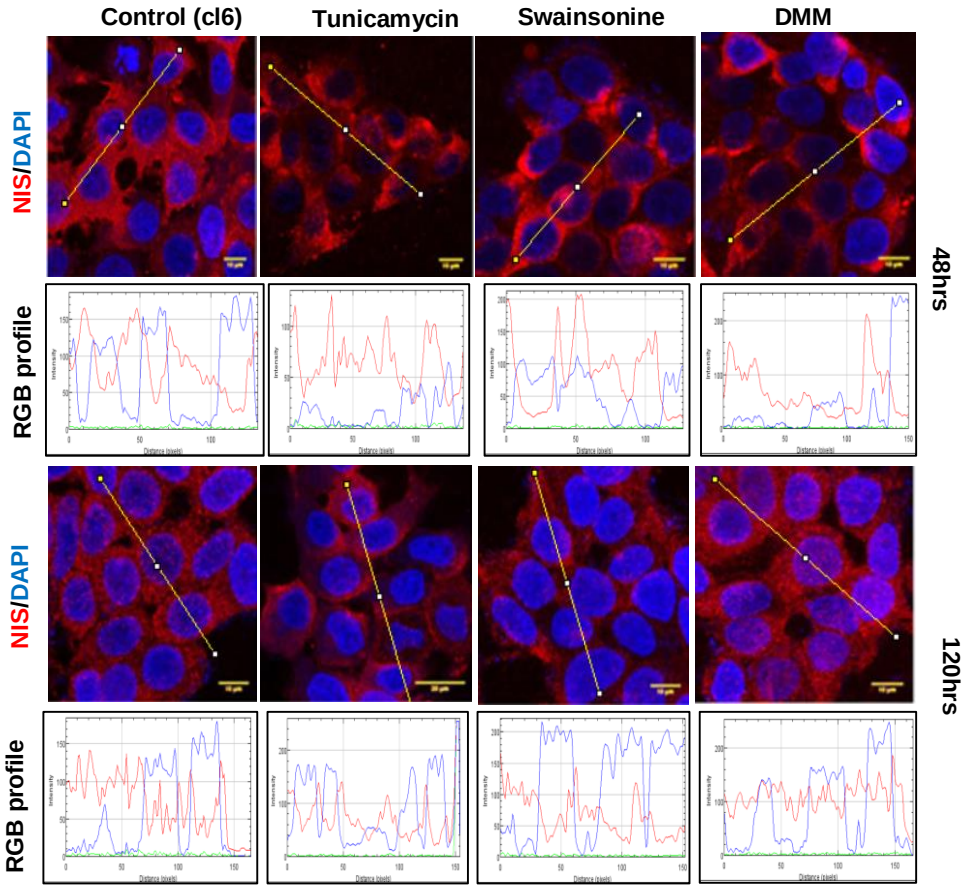

S4B

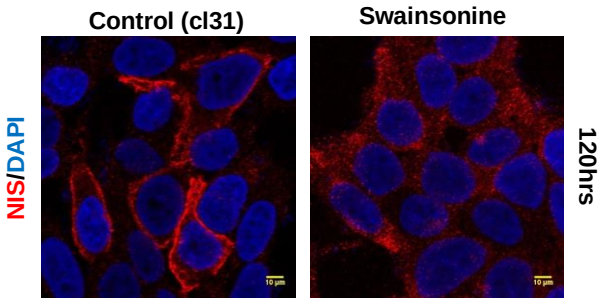

Figure S4: The effect glycosylation inhibitors on NIS localization in cytoplasmic clones, and the action of swainsonine over 120 hours in cl31. NIS localization in cytoplasmic clone is not affected by glycosylation inhibitor treatment and swainsonine can take down membrane expression of NIS over 120 hours **S4A.** IF images showing the localization of NIS (red) in response to glycosylation inhibitors tunicamycin, DMM and swainsonine at 48 and 120 hours in cytoplasmic clone. **S4B**. IF images showing the delayed action of swainsonine on altering NIS (red) localization over 120 hours. The scale bar represents 10µm

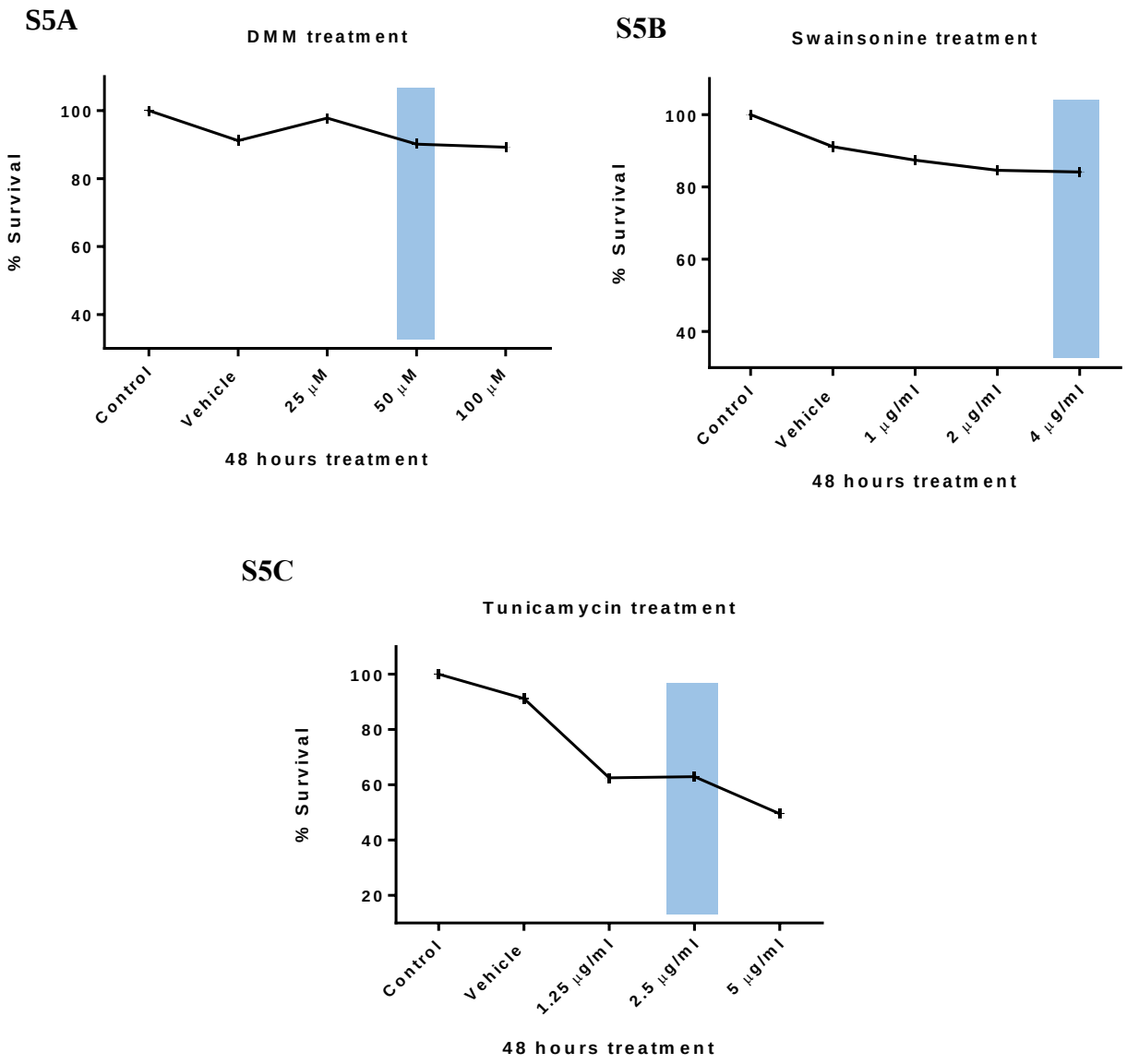

Figure S5: Cytotoxicity of glycosylation inhibitors on MCF-7 cells. The glycosylation pathway inhibitors used are not cytotoxic to MCF-7 cells**. S5A-C:** Graph showing the results from MTT assay, revealing that the selected dose of each drug for the study (highlighted in blue), lies below IC50.

S6A

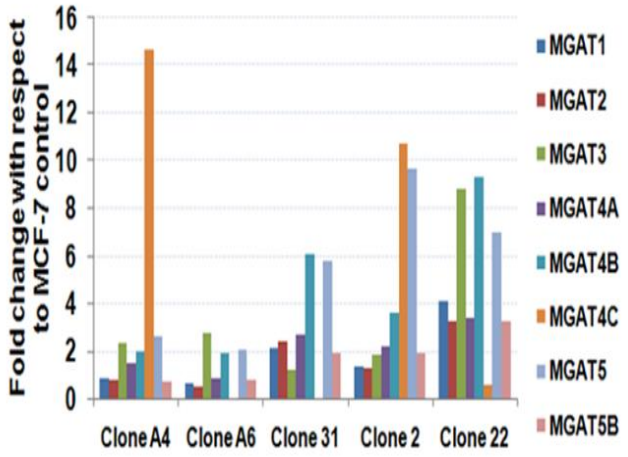

S6B

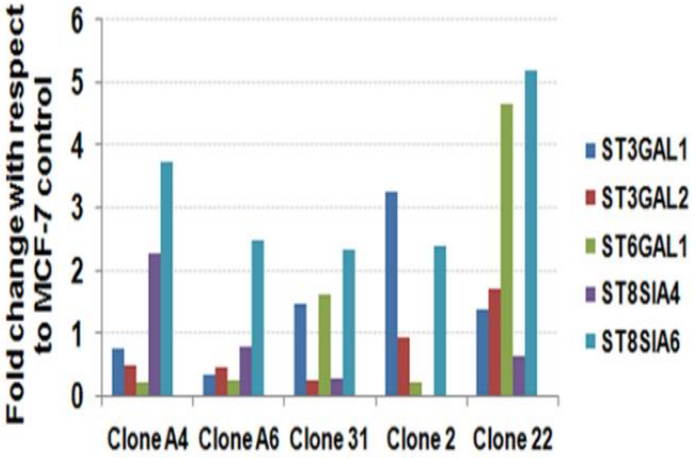

S6C

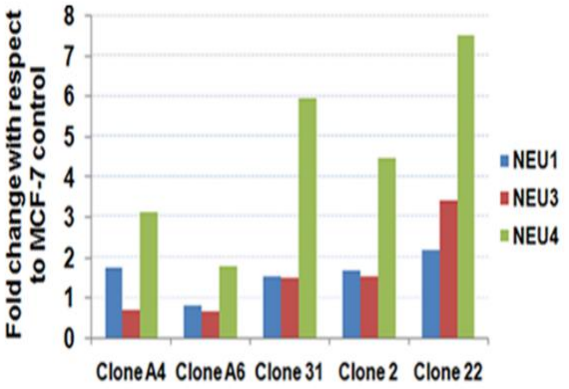

Figure S6: Expression of various class of glycosylation enzyme coding genes across clonal models and MCF-7 baseline cell. Differential expression of various class of glycosylation enzyme coding genes across membrane and cytoplasmic clone w.r.t to baseline cells **S6A.** Chart showing fold change for various mannosyl transferase enzyme coding genes in membrane and cytoplasmic clones with respect to baseline MCF-7 cell. **S6B.** Chart showing differential expression profile of sialidases enzyme coding genes. **S6C.** Chart showing differential expression profile of neuramindase enzyme coding genes.

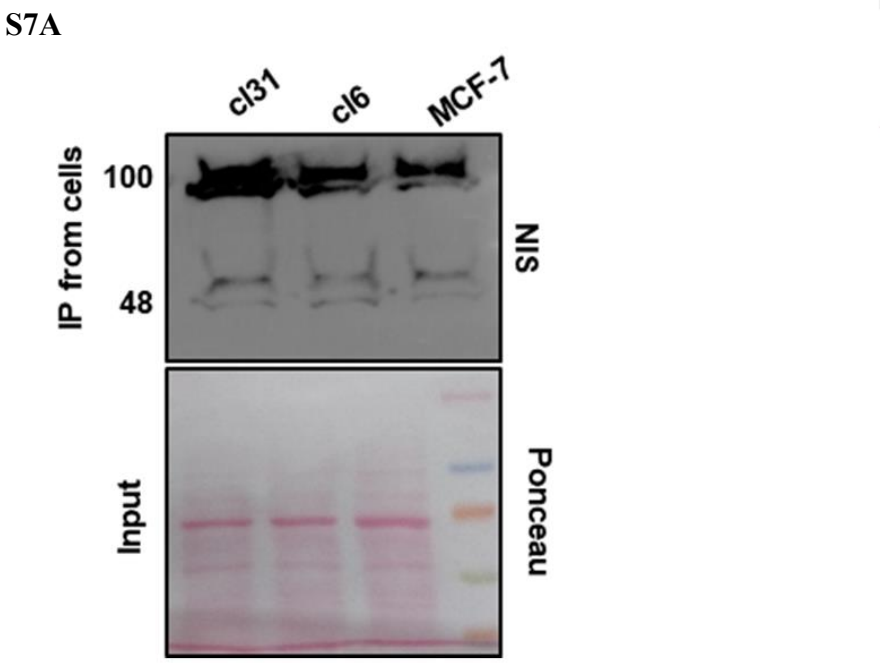

Figure S7: NIS western blot showing effective pull down of NIS from the clonal cell models. Immunoprecipitation of NIS from the different cell lineages reveals that cl31 possess the highest amount of 100kDa fraction of NIS. **S7A:** Western blot showing the staining of NIS from the IP sample, across the different cell types. Ponceau staining was used as a loading control from input samples.

Table S1: Karyotype analysis of MCF-7 derived stable cell models of differential NIS localization.

Cell line	MCF-7 parent	cl31	cl6
Ploidy	Triploidy	Triploidy	Triploidy
Similar abnormalities	• Derivative chromosome 1 due to inversion and duplication of chromosome • Isochromosomes of q arm of chromosome 7 and 11	• Derivative chromosome 1 due to inversion or duplication of chromosome • Isochromosomes of q arm of chromosome 7 and 11	• Derivative chromosome 1 due to inversion or duplication of chromosome • Isochromosomes of q arm of chromosome 7 and 11
Differential abnormalities	Deletion in p/q arm of chromosome 1,2,3,6,11,17 Extra copies of chromosomes 7,8,9,10,11,13,14,15,16,17	Deletion in p/q arm of chromosome 1,6,8,11,17 Extra copies of chromosomes 4,5,7,8,9,10,11,13,15,16,17,20,22	Deletion in p/q arm of chromosome 1,2,3,6,8,11,17 Extra copies of chromosomes 4,5,7,8,9,10,11,13,14,15,16,17,20

Table S1: Clonal heterogeneity among MCF-7 clones based on karyotype differences. GTG banding pattern has been used to evaluate the chromosome structures and numbers.